A COMPACT X-BAND RECEIVER FRONT-END MODULE BASED ON LOW TEMPERATURE CO-FIRED CERAMIC TECHNOLOGY

Z. Wang, P. Li, R. Xu, and W. Lin

School of Electronic Engineering
University of Electronic Science and Technology of China
Chengdu, Sichuan 610054, P. R. China

Abstract—This letter presents a compact low temperature co-fired ceramic (LTCC) receiver front-end module integrating 9 building blocks. The receiver is a twice-frequency-conversion front-end module with image rejection, works at X-band, consists of an X-band embedded image rejection band-pass filter (BPF), an L-band multilayer image rejection quasi-ellipitc BPF, two monolithic microwave integrated circuit (MMIC) low noise amplifiers (LNAs), two intermediate frequency (IF) amplifiers, two mixers, a IF BPF, and some lumped passive components. All MMICs are mounted into pre-making cavities in the three layers LTCC substrate of the top surface, and the interconnection between MMICs and surface microstrip-line is established by bond wires. A multilayer five-pole Chebyshev interdigital BPF is developed as the first image rejection filter, and a four-pole quasi-elliptic BPF composed of stepped-impedance hairpin resonator and miniaturized hairpin resonators that can be coupled through the apertures on the common ground plane is proposed for as the second image rejection filter. The developed X-band receiver front-end module is fabricated using twenty layers LTCC dielectric substrate, which has a compact size of $30 \times 20 \times 20 \, \text{mm}^3$ (including the metal cavity). The measured receiver gain and noise figure are more than 32 dB and less than 4 dB, respectively. The first and second image rejection is better than 28 dB and 40 dB, respectively. Compared with conventional receiver front-end module using hybrid microwave integrated circuit (HMIC) technology, the proposed receiver module not only has compact size, but also has good performance.

Corresponding author: Z. Wang (zgwang@ee.uestc.edu.cn).

1. INTRODUCTION

The tremendous growth of radars, electronic antagonism technologies and wireless communications require low manufacturing cost, excellent performance and high level of integration for transmitter and receiver modules, or transceiver modules [1–7, 22–28]. The multilayer low temperature co-fired ceramic (LTCC) technology offers a solution for the requirements. Lately LTCC has become an attractive material system for innovative designs, due to its attributes of low volume production cost, multilayer fabrication capability, low-loss transmission lines and high quality factor passive devices for microwave and millimeter-wave circuits. The use of multilayer LTCC technology makes it possible to integrate active devices (such as power amplifiers, low noise amplifiers, mixers, intermediate frequency amplifiers and transmitting/receiving diversity switches) and buried passive devices (such as lowpass filters, band-pass filters, baluns, diplexers, matching networks and even antennas) into a package. Numerous publications [8–15] have dealt with the development of three dimension (3-D) LTCC filters and modules.

In this letter, a LTCC-based X-band receiver front-end module is designed, and fabricated using twenty layers LTCC dielectric substrate, which is only $30 \times 20 \times 20$ mm^3 (including the metal cavity). The module comprises an X-band image rejection BPF, an L-band image rejection BPF, two MMIC LNAs, two IF amplifiers, two mixers, an IF BPF, and some lumped passive components. The X-band and L-band BPF are all buried in the LTCC substrate for size reduction, and realized by a multilayer five-pole Chebyshev interdigital BPF and a four-pole quasi-elliptic BPF composed of stepped-impedance hairpin resonator and miniaturized hairpin resonators, respectively. The integrated receiver front-end module demonstrates excellent performances: The gain and noise figure are more than 32 dB and less than 4 dB, respectively. The first and second image rejection are better than 28 dB and 40 dB, respectively.

2. DESIGN OF COMPONENTS

The block diagram of the X-band receiver front-end module to be developed in this paper is shown in Fig. 1. The receiver is a twice-frequency-conversion front-end module with image rejection, and the module is composed of an X-band image rejection BPF, an L-band image rejection BPF, two MMIC LNAs, two IF amplifiers, two mixers, an IF BPF, and some lumped passive components. The X-band BPF and L-band BPF are buried in the LTCC substrate for compact size,

while the two MMIC LNAs, two IF amplifiers, two mixers, an IF BPF, and lumped passive components are mounted on the top and bottom surface of the LTCC substrate. The X-band and L-band BPF are realized by a multilayer five-pole Chebyshev interdigital BPF and a four-pole quasi-elliptic BPF composed of stepped-impedance hairpin resonator and miniaturized hairpin resonators, respectively. More details about the two BPF will be revealed in the following.

2.1. X-band BPF

The X-band BPF (as shown in Fig. 1) is used reject image signals (6.76–7.76 GHz) and out-of-band spurious signals. A multilayer five-pole Chebyshev interdigital BPF was chosen for its small size and easy integration. Figs. 2(a) and (b) shows the top and cross-section views of the X-band embedded LTCC BPF, respectively. The LTCC substrate has twenty layers Ferro A6-M LTCC substrate for the whole module integration, of which the relative permittivity is about 5.7, loss tangent is 0.003, and thickness of each layer is 0.094 mm. The BPF is embedded into upper-four layers, Grid-ground structure is buried at the fifth layer, as a ground of the microstrip line. The BPF's structure is similar to conventional interdigital filters in planar circuits, but all of resonators are embedded into LTCC substrate, and placed at different layers. The amount of coupling (coupling coefficient) for each resonator is controlled by the offset between them, and the external quality factor Q_e is decided by the position of input/output broadside coupled microstrip line. As a result, the radiation loss and volume of this filter are reduced remarkably.
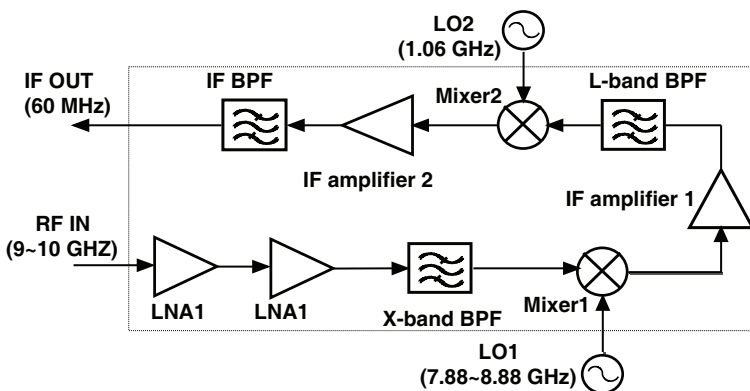

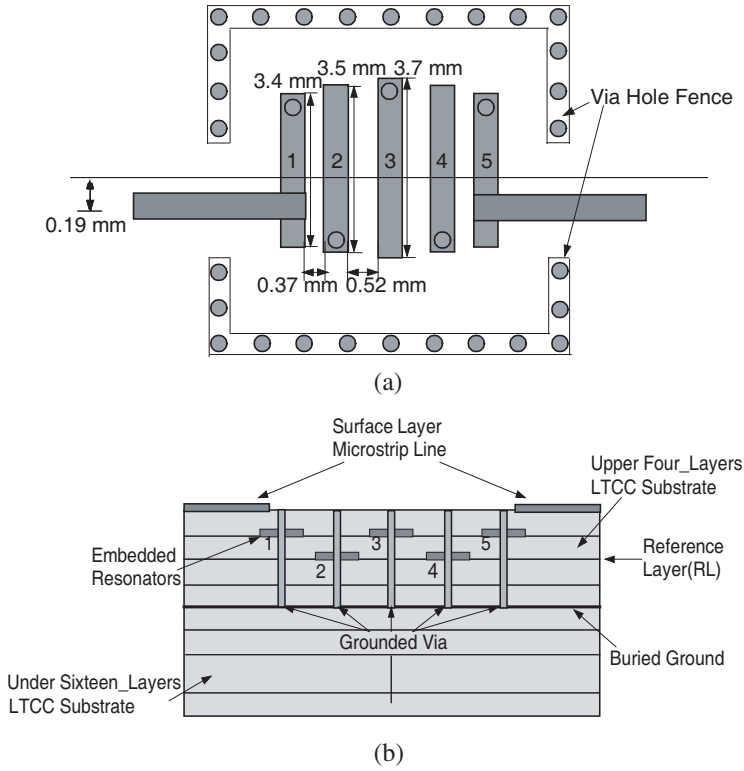**Figure 1.** The block diagram of the X-band receiver front-end module.

Figure 2. Configuration of the X-band embedded LTCC BPF: (a) Top view. (b) Cross section.

The BPF should be designed to meet the following specifications: (1) center frequency: 9.5 GHz; (2) bandwidth: 1 GHz; (3) suppression is better than 25 dB at 6.76–7.76 GHz. The design parameters such as the coupling coefficients and the external quality factor can be theoretically calculated based on the element values of a five-pole low pass prototype filter [16]. Relationship between physical dimension and parameter (coupling coefficients and external quality factor) is established using Ansoft Corporation's full wave electromagnetic (EM) High Frequency Structure Simulator (HFSS) simulator. After optimization, the structure dimensions is confirmed, as shown in Fig. 2. Further more, a fence structure, which is formed by metal-filled vias, is set around the BPF. This is based on considerations of electromagnetic interference (EMI) between BPF and other circuits in the module. Fig. 3 shows the simulated S parameters of the X-band BPF. The filter exhibits good performance: Passband insertion loss is less than

2.2 dB (1.62 dB at 9.5 GHz); the return loss is better than −19.8 dB over the operating bandwidth; in the stop-band, rejection of 44.7 dB is achieved at 6.76 GHz, and 32.7 dB is achieved at 7.76 GHz. Suppression for image signals is satisfied.

2.2. L-band BPF

The L-band BPF (as shown in Fig. 1) is used reject image signal (1 GHz) and some spurious signals, especially the local oscillator (LO) signals (7.88–8.88 GHz). A four-pole quasi-elliptic BPF composed of stepped-impedance hairpin resonator and miniaturized hairpin resonators [17–19] are designed for this application, due to its compactness and its 3-D interconnect feature between the devices on the top and bottom of the LTCC board. A high level of compactness can be achieved by stacking four resonators vertically coupled through three coupling apertures etched on a common ground plane with tapped-line input/output. The 3-D overview of the fourpole quasi-elliptic BPF is shown in Fig. 4. The LTCC substrate has twenty layers Ferro A6-M LTCC substrate whose relative permittivity is about 5.7, loss tangent is 0.003, and thickness of each layer is 0.094 mm. The filter consists of two types of resonators. One is the stepped-impedance hairpin resonator and the other is the miniaturized hairpin resonator. In addition, the tapped-lines are used as the input/output coupling, for they can generate two independent transmission zeros in the stop-band [20], and increase the selectivity and out-of-band rejection of the filter. The stepped-impedance hairpin resonators and the miniaturized hairpin resonators are located inner sides of the LTCC substrate. Cross-coupling among the resonators is established with the aid of apertures on the common ground plane.

The four resonators are designated as resonators 1–4, as shown in Fig. 4. Resonators 1 and 4 represent the stepped-impedance hairpin resonator. Resonators 2 and 3 represent the miniaturized hairpin resonator, which are composed of a section of a folded transmission line and a section of a coupled line with open-end termination. The coupling between resonators 1 and 2 is identical to that between resonators 3 and 4. So, there are three basic coupling structures in the proposed filter structure. The coupling between resonator 1 and 4 is electric coupling, which is decided by the two side apertures on the common ground plane. The coupling between resonators 2 and 3 is magnetic coupling, which is controlled by the middle aperture on the common ground plane. The coupling between resonators 1 and 2, or between resonators 3 and 4, is mixed coupling including electric and magnetic coupling, which is established by the space between resonators.
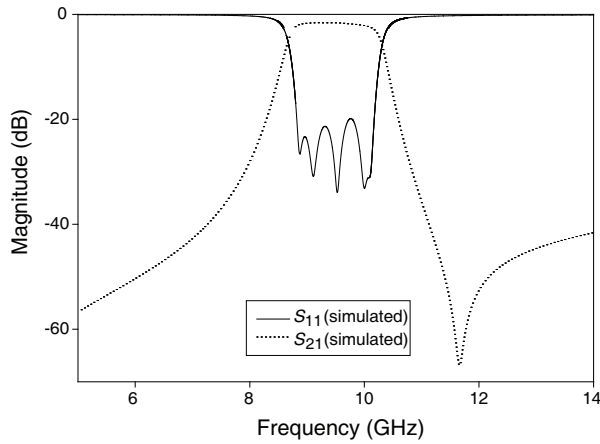
Figure 3. The simulated S parameters of the X-band embedded LTCC BPF.
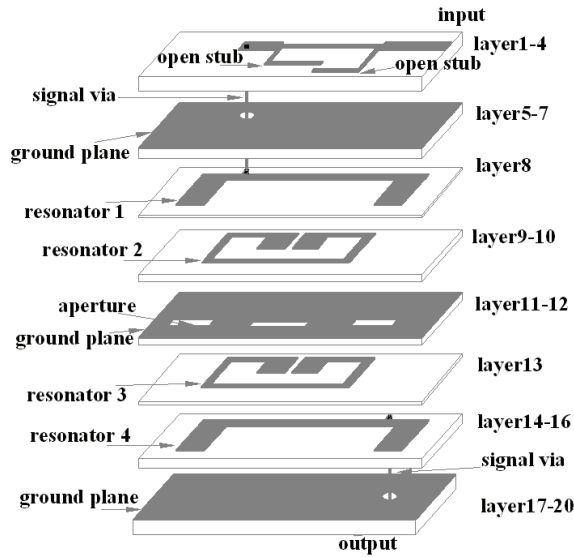

Figure 4. The 3-D overview of the four-pole quasi-elliptic BPF.

The L-band BPF should be designed to meet the following specifications: (1) center frequency: 1.14 GHz; (2) bandwidth: 0.08 GHz; (3) suppression is better than 25 dB at 1 GHz, is better than 20 dB at 7.88–8.88 GHz. The design parameters such as the coupling coefficients and the external quality factor can be theoretically

calculated based on the lumped-element values of a four-pole low pass prototype filter [21]. Relationship between physical dimension and parameter (coupling coefficients and external quality factor) is established using Ansoft Corporation's full wave electromagnetic (EM) High Frequency Structure Simulator (HFSS) simulator. After analyzing and optimizing the BPF using Ansoft HFSS, the structure dimensions is confirmed. A fence structure that is formed by metal-filled vias is also set around the BPF for rejecting EMI, like the X-band BPF. The simulated results are shown in Fig. 5(a). It can be
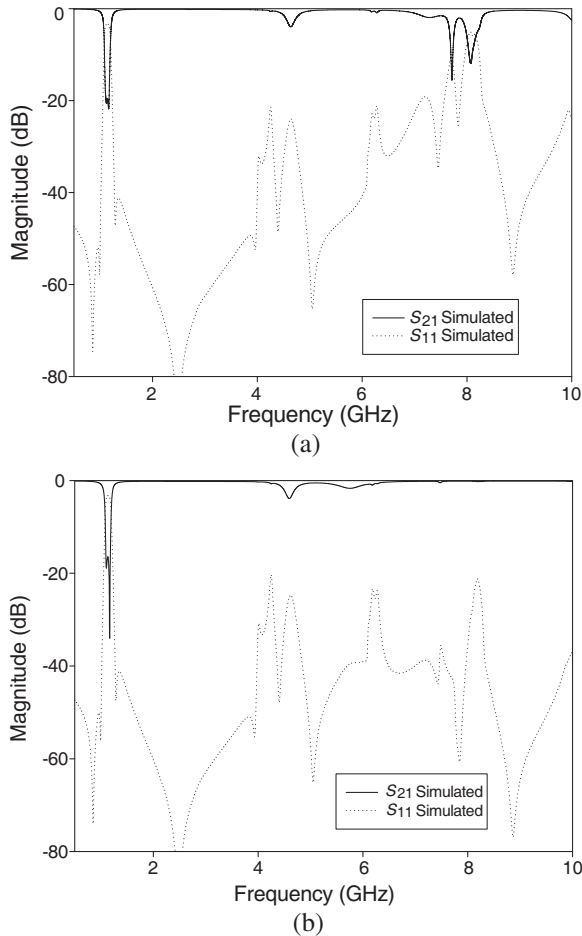

Figure 5. The simulated S parameters of the four-pole quasi-elliptic BPF: (a) Without open-stubs. (b) With open-stubs.

seen from the Fig. 5(a) that the suppression of 7.88–8.88 GHz is not meted for parasitic pass-band of the filter. So, two open-stubs are connected at the input port for better rejection. Fig. 5(b) shows the simulated S parameters of the L-band BPF with open-stubs. The filter exhibits good performance: Passband insertion loss is less than 4.5 dB (3.4 dB at 1.12 GHz); the return loss is better than -16.2 dB over the operating bandwidth; in the stop-band, rejection of 53 dB is achieved at 1 GHz, and more than 21 dB suppression is achieved at 7.88–8.88 GHz. Suppression for image signal and LO signals are satisfied. It can be clearly observed that there are four transmission zeros: 0.85 GHz, 1 GHz, 1.28 GHz and 2.48 GHz. The transmission zeros 1 GHz and 1.28 GHz are caused by the cross coupling between resonator 1 and 4. The transmission zeros 0.85 GHz and 2.48 GHz are caused by the tapped-line input/output coupling. The effect can increase the rejection in the stopband.
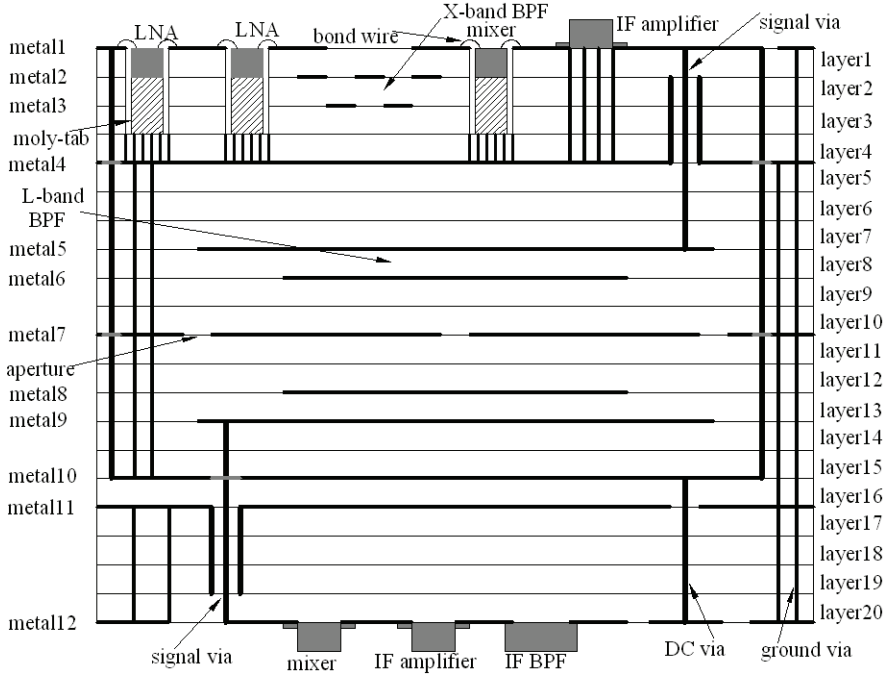

Figure 6. The cross-section view of the receiver front-end module.

3. INTEGRATION OF THE RECEIVER FRONT-END MODULE

The cross-section view of the X-band receiver front-end module is shown in Fig. 6. It has been designed on twenty layers Ferro A6-M LTCC substrate (relative permittivity 5.7, loss tangent 0.003, and thickness of each layer 0.094 mm), which consist of twenty dielectric layers and twelve metal layers. The metal layers 1 and 12 are for RF circuits, IF circuits, and required dc bias. The metal layers 2, 3, 5, 6, 8 and 9 are for filter resonators. The metal layer 10 is for dc circuits. The ground planes are located on the metal layers 4, 7 and 11. Two MMIC LNAs and one MMIC mixer are embedded into pre-making cavities of the LTCC substrate and mounted on the fourth layer substrate with an elevated ground plane, which is connected to ground plane through
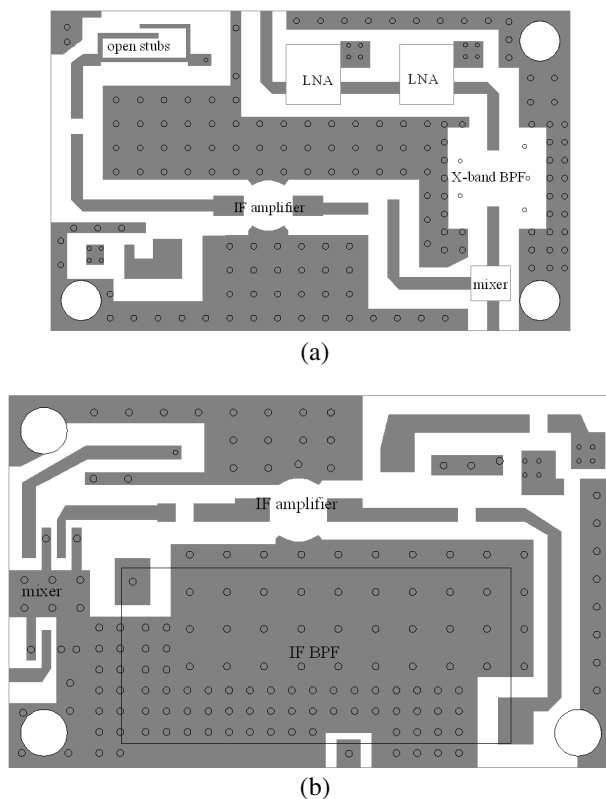

(a)

(b)

Figure 7. (a) Top and (b) bottom views of the receiver front-end module.

stacked ground vias. In order to achieve that the surface of MMICs are coplanar with the surface of the substrate and good electrical performance, the MMICs are attached to a 0.2 mm thick molybdenum heat spreader (moly-tab) which is then attached to the ground plane. Two IF amplifiers, one surface mounted (SMT) mixer, an IF BPF and required components for supplying dc bias, are all mounted on the top and bottom surface layers. The proposed multilayer five-pole Chebyshev interdigital BPF is embedded into upper-four layers, which is connected with MMICs by bond wires. The proposed four-pole quasi-elliptic BPF is embedded into middletwelve layers through connection of via transitions.
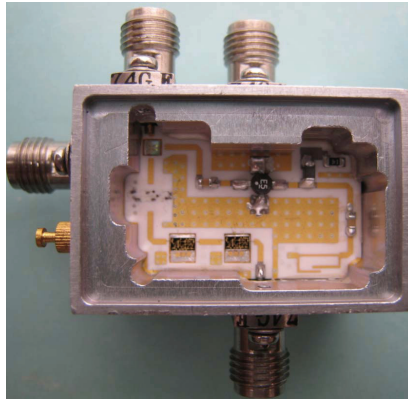
(a)
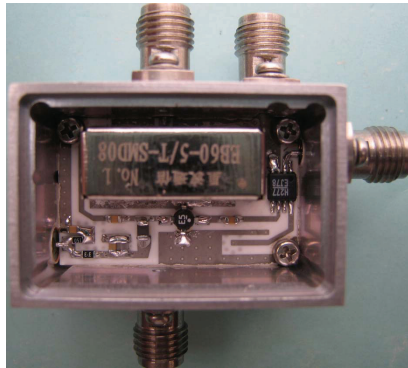
(b)

Figure 8. (a) Top and (b) bottom of the fabricated receiver front-end module.
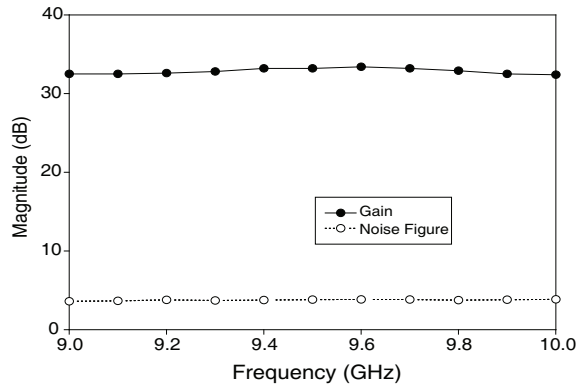
Figure 9. The measured gain and noise figure of the receiver front-end module.

Figure 7 shows top and bottom views of the fabricated receiver front-end module before attaching devices. The size of the designed LTCC substrate is $26 \times 16 \times 2\,\text{mm}^3$. The MMICs, packaged active devices, and lumped passive device are attached on the LTCC substrate using silver epoxy, and the LTCC substrate is mounted in a metal cavity, as shown in Fig. 8. The total receiver front-end module has a compact size of $30 \times 20 \times 20\,\text{mm}^3$ (including the metal cavity).

Figure 9 shows part performance characteristics of the fabricated receiver front-end module. In operating frequency range, the measured receiver gain and noise figure are more than 32 dB and less than 4 dB, respectively. The first image rejection (6.76–7.76 GHz) is better than 28 dB. In addition, the second image rejection (1 GHz) is better than 40 dB.

4. CONCLUSION

In this paper, a compact X-band multilayer LTCC-based receiver front-end module has been fabricated and measured. In addition, a five-pole Chebyshev interdigital BPF and a four-pole quasi-elliptic BPF has been designed as the first and second image rejection filter. The developed filters and other devices have been combined together, leading to a highly integrated receiver front-end module with high performance. The total receiver front-end module has a compact size of $30 \times 20 \times 20\,\text{mm}^3$ (including the metal cavity). The measured receiver gain and noise figure are more than 32 dB and less than 4 dB, respectively. The first and second image rejection is better than 28 dB and 40 dB, respectively.

ACKNOWLEDGMENT

REFERENCES

1. Lim, K., S. Pinel, M. F. Davis, A. Sutono, C. H. Lee, D. Heo, A. Obatoynbo, J. Laskar, E. M. Tentzeris, and R. Tummala, "RF-system-on-package (SOP) for wireless communications," *IEEE Microwave Mag.*, Vol. 3, No. 1, 88–99, March 2002.

2. Bae, J. H., W. K. Choi, J. S. Kim, G. Y. Choi, and J. S. Chae, "Study on the demodulation structure of reader receiver in a passive RFID environment," *Progress In Electromagnetics Research*, PIER 91, 243–258, 2009.

3. Kim, J.-H., Y.-H. You, K.-I. Lee, and J.-H. Yi, "Pilot-less synchronization receiver for UWB-based wireless application," *Progress In Electromagnetics Research*, PIER 83, 119–131, 2008.

4. Chan, Y. K. K., B. K. Chung, and H. T. Chuah, "Transmitter and receiver design of an experimental airborne synthetic aperture radar sensor," *Progress In Electromagnetics Research*, PIER 49, 203–218, 2004.

5. Ma, T.-G., C.-J. Wu, and C.-F. Chou, "An impulse-radio-based ultrawideband RF front-end module with a new multilayered microwave sampler," *Progress In Electromagnetics Research*, PIER 86, 1–18, 2008.

6. Li, S., S. L. Zheng, X. M. Zhang, and X. F. Jin, "A compact photonic microwave receiver integrated with dielectric resonator antenna," *Journal of Electromagnetic Waves and Applications*, Vol. 22, No. 11–12, 1547–1555, 2008.

7. Alivizatos, E. G., M. N. Petsios, and N. K. Uzunoglu, "Towards a range-doppler UHF multistatic radar for the detection of non-cooperative targets with low RCS," *Journal of Electromagnetic Waves and Applications*, Vol. 19, No. 15, 2015–2031, 2005.

8. Wang, G. Q., M. Van, F. Barlow, and A. Elshabini, "An interdigital bandpass filter embedded in LTCC for 5 GHz wireless LAN applications," *IEEE Microw. Wireless Compon. Lett.*, Vol. 15, No. 5, 357–359, May 2005.

9. Yeung, L. K. and K. L. Wu, "A compact second-order LTCC bandpassfilter with two finite transmission zeros," *IEEE Trans. Microw. Theory Tech.*, Vol. 51, No. 2, 337–341, February 2003.

10. Lee, J.-H., N. Kidera, G. DeJean, S. Pinel, J. Laskar, and

M. M. Tentzeris, "A v-band front-end with 3-D integrated cavity filters/duplexers and antenna in LTCC technologies," *IEEE Trans. Microw. Theory Tech.*, Vol. 54, No. 7, 2925–2937, July 2006.

11. Lee, C. H., A. Sutono, S. Han, K. Lim, S. Pinel, J. Laskar, and E. M. Tentzeris, "A compact LTCC-based Ku-band transmitter module," *IEEE Trans. Adv. Packag.*, Vol. 25, No. 3, 374–384, August 2002.

12. Yeung, L. K., J. Wang, Y. Huang, S. C. Lee, and K. L. Wu, "A compact LTCC Bluetooth system module with an integrated antenna," *Int. J. RF Microw. Comput. Aided Eng.*, Vol. 16, No. 3, 238–244, February 2006.

13. Ko, Y. J., J. Y. Park, J. H. Ryu, K. H. Lee, and J. U. Bu, "A miniaturized LTCC multi-layered front-end module for dual band WLAN (802.11a/b/g) applications," *IEEE MTT-S Int. Microw. Symp. Dig.*, 563–566, June 2004,

14. Weng, C. C., C. F. Chang, and S. J. Chung, "Development of a compact low- remperature co-fired ceramic antenna front-end module," *IEEE Trans. Microw. Theory Tech.*, Vol. 56, No. 11, 2483–2492, November 2008.

15. Baras, T. and A. F. Jacob, "Integrated LTCC synthesizer and signal converter modules at K-band," *IEEE Trans. Microw. Theory Tech.*, Vol. 57, No. 1, 71–79, January 2009.

16. Hong, J. S. and M. J. Lancaster, *Mircrostrip Filters for RF/Microwave Applications*, Wiley, New York, 2001.

17. Hong, J. S. and M. J. Lancaster, "Theory and experiment of novel microstrip slow-wave open-loop resonator filters," *IEEE Trans. Microw. Theory Tech.*, Vol. 45, No. 12, 2358–2365, December 1997.

18. Sagawa, M., K. Takahashi, and M. Makimoto, "Miniaturized hairpin resonator filters and their application receiver front-end MIC's," *IEEE Trans. Microw. Theory Tech.*, Vol. 37, No. 12, 1991–1997, November 1989.

19. Djaiz, A. and T. A. Denidni, "A new compact microstrip two-layer bandpass filter using aperture-coupled SIR-hairpin resonators with transmission zeros," *IEEE Trans. Microw. Theory Tech.*, Vol. 54, No. 5, 1929–1936, May 2006.

20. Kuo, J.-T. and E. Shih, "Microstrip stepped impedance resonators bandpass filter with an extended optimal rejection bandwidth," *IEEE Trans. Microw. Theory Tech.*, Vol. 51, No. 5, 1554–1559, May 2003.

21. Levy, R., "Filters with single transmission zeros at real or

imaginary frequencies," *IEEE Trans. Microw. Theory Tech.*, Vol. 24, No. 4, 172–181, April 1976.

22. Zhao, X. and K. Huang, "Calculation of probability distribution of maximal received power of electronic receiver in lighting electromagnetic environment," *Journal of Electromagnetic Waves and Applications*, Vol. 19, No. 2, 221–230, 2005.

23. Guo, Y. and R. Xu, "Ultra-wideband power splitting/combining technique using zero-degree left-handed transmission lines," *Journal of Electromagnetic Waves and Applications*, Vol. 21, No. 8, 1109–1118, 2007.

24. Jiang, B. T. and J. F. Mao, "A good performance design for integrating three antennas in a dual SIM mobile phone for GSM/DCS/Bluetooth operations," *Journal of Electromagnetic Waves and Applications*, Vol. 22, No. 14–15, 1943–1954, 2008.

25. Guo, Y. and R. Xu, "Planar metamaterials supporting multiple left-handed modes," *Progress In Electromagnetics Research*, PIER 66, 239–251, 2006.

26. Chou, H. T., L. R. Kuo, and W. J. Liao, "Characteristic evaluation of an active patch antenna structure with an embedded LNA module for GPS reception," *Journal of Electromagnetic Waves and Applications*, Vol. 21, No. 15, 599–614, 2007.

27. Guo, Y., Y. Xu, L. Xia, and R. Xu, "Efficient optimization of a Ka-band branch waveguide power divider," *Journal of Electromagnetic Waves and Applications*, Vol. 22, No. 1, 17–26, 2008.

28. Fakoukakis, F. E., S. G. Diamantis, A. P. Orfanides, and G. A. Kyriacou, "Development of an adaptive and a switched beam smart antenna system for wireless communication," *Journal of Electromagnetic Waves and Applications*, Vol. 20, No. 3, 399–408, 2006.